

Modeling of Jets from Comet Hale–Bopp (C/1995 O1): Observations from the Vainu Bappu Observatory

R. Vasundhara and Pavan Chakraborty

Indian Institute of Astrophysics, Bangalore 500034, India

E-mail: rvas@iiap.ernet.in

Received June 11, 1998; revised January 4, 1999

1. INTRODUCTION

Jet and shell structures from Comet Hale–Bopp during the period October 1996 to October 1997 using data from the Vainu Bappu Observatory are modeled. Evolution of jet and shell structures during the period of observations could be attributed to activity from sources near $+65^\circ$, $+35^\circ$, $+5^\circ$, -5° , -35° , -65° in latitude. Although no deliberate attempt was made to place the sources at symmetric latitudes, the best fit shows a remarkable symmetry. Due to changing solar illumination geometry, while only the southern sources were apparently active during 1996, most of the sources appeared active in February 1997 and October 1997. In the 10 April image, under a near pole-on solar illumination, curiously, only the sources at $+65^\circ$, $+5^\circ$, and -5° appear to be active and not the source at $+35^\circ$. Pole positions which gave a reasonably good fit to the observed sets of shells varied from 260° to 290° in right ascension and -50° to -65° in declination. Around 10 April, while the gas production from the equatorial sources is expected to be low due to near grazing incidence of the Sun light, the fractional area of the high latitude source is limited for a spherically symmetric nucleus. To explain the well-defined shells due to rotation of the jets, we assume that the source at $+65^\circ$ occupies 10% of the longitude belt and 10° in latitude. Assuming a radius of 35 km for the comet corresponding to the upper limit of H. A. Weaver and P. L. Lamy (1999, *Earth Moon Planets*, in press) and Z. Sekanina (1999b, *Earth Moon Planets*, in press), the area of 56 km^2 for this source could account for 29% of the observed total production rate of $4.0 \times 10^{30} \text{ molecules s}^{-1}$ by D. G. Schleicher *et al.* (1997, *Bull. Am. Astron. Soc.* 29, 1033). The intricate shell patterns during February–May 1997 could not be exactly replicated using the model of a single nucleus. Complexity of the shell structures can be better explained using the binary model of Comet Hale–Bopp suggested by Sekanina (1999a, *Earth Moon Planets*, in press; 1998b, *Astrophys. J.* 509, L133–L136) with sizes of 70 and 30 km across. Approximate estimates of the longitude of the sources active between February and May 1997 are presented. The lower limits on the dust to gas mass production ratio are estimated to be, 4.8 ± 1.1 , 3.4 ± 1.0 , and 6.2 ± 1.3 on 18 February, 10 April, and 2 May, 1997, respectively.

© 1999 Academic Press

Key Words: comets, Hale–Bopp; imaging; dust ejection, dust jets; production rates: gas, dust.

Beginning in May 1996, several observers reported multiple jets from Comet Hale–Bopp. Manzini *et al.* (1996) reported several secondary jets in August 1996, which gave the comet the appearance of a porcupine. Sekanina and Boehnhardt (1997, 1999) interpreted jet pairs (one pair per source) as the boundaries of fan-shaped formations described by dust ejected from the sources continually between local sunrise and sunset. To explain the observations during May–November 1996, they proposed two models, one with six sources and a spin axis undergoing a complex motion and another with a fixed spin axis and a large diurnal dust ejection fluctuations for one of the jets. Sekanina (1998a) used Monte Carlo computer simulation to show that the dust source producing the south westerly halo in the time-resolved image sequences by Jorda *et al.* (1999) is located at $+55^\circ$ and derived the pole positions. Samarasinha *et al.* (1999) constrained the direction of the spin axis of the nucleus referred to the ecliptic. Vasundhara *et al.* (1999) fitted the jets and shells in 12 images of the comet obtained at the observatory of the Naturwissenschaftlicher Verein Osnabrück during September 1996 to May 1997 to derive the latitude of the jet sources and pole positions. We attempt here to model the jets using the observations from the Vainu Bappu Observatory from October 1996 to October 1997 to determine the location of the active regions and the pole positions.

2. OBSERVATIONS AND DATA PROCESSING

The observations (filter imaging) of Comet Hale–Bopp were carried out at the prime focus ($f/3.3$) of the 2.34-m telescope and at the cassegrain focus ($f/13$) of the 1.02-m telescope. The detectors used were the TK1024 Photometric liquid nitrogen cooled CCD at the 2.34-m telescope and the 384×576 Thompson chip Photometric liquid nitrogen cooled CCD at the 1.02-m telescope. Images taken through an R-filter were selected for investigating the dust shells and jets from this comet. Table I gives the log of these selected observations. The radial

TABLE I
Journal of Observations

| Date | Time (UT) | Exposure | Telescope | Image scale arcsec/pixel | Phase (deg) |
|--------------|-----------|----------|-----------|-----------------------------|----------------|
| 1996 Oct. 06 | 13 : 55 | 20 s | 234 cm | 0.60 | 19.4 |
| 1996 Nov. 04 | 13 : 30 | 30 s | 234 cm | 0.60 | 16.9 |
| 1997 Feb. 18 | 00 : 03 | 2 s | 234 cm | 0.60 | 35.4 |
| 1997 Apr. 10 | 13 : 32 | 7 s | 102 cm | 0.36 | 43.3 |
| 1997 May 02 | 13 : 33 | 20 s | 102 cm | 0.36 | 29.2 |
| 1997 Oct. 09 | 22 : 12 | 10 s | 234 cm | 0.60 | 18.6 |

and rotational shift algorithm by Larson and Sekanina (1984) was applied on the bias and flat-field corrected images to suppress the strong radial intensity gradient in the coma to enhance smaller fluctuations like the jets and the shells. A rotation of $\pm 10^\circ$ around the comet centroid in the rotational shift algorithm seemed suitable for these images. The images were then scaled over the comet's intensity range saturating the brighter field stars to obtain the best gray scale. These operations were carried out using the IRAF packages and the XV 3.10.

3. COMPUTATION OF THE TRACK OF THE DUST GRAINS IN THE JETS

Our computer simulations are based on the basic concepts introduced by Sekanina (1981a, 1981b, 1991) and Sekanina and Larson (1984). The computer code predicts the loci of the dust grains as seen projected on the sky plane relative to the comet at any instant of time.

3.1. Velocity and Acceleration of the Grains

The sources are assumed to emit jets of gas and dust from local sunrise to sunset. Diurnal changes in production rates from the sources are neglected. A mean period of 11.34 h reported by Licandro *et al.* (1998), which is close to the value of $11.35 \pm .04$ h reported by Jorda *et al.* (1999) is used in the present analysis. On leaving the nucleus radially, the dust grains move under the combined force of solar radiation pressure and solar gravity. We neglect the gravitational force of the nucleus. The velocity v_{gr} and acceleration α due to solar radiation pressure depend on the size and nature of the grains and the heliocentric distance. In the absence of the knowledge of the nature of the grains, we estimated α using the relation

$$\alpha = \beta g_{sun(1)}/r^2, \quad (1)$$

where β is the ratio of the force due to solar radiation pressure on the grain to the gravitational force and $g_{sun(1)}$ is the acceleration due to solar gravity at one AU ($0.6 \times 10^{-5} \text{ km s}^{-2}$). The velocity attained by the grains by the time the dust and gas get decoupled from each other within a few nuclear radii (Probstein 1969) was calculated using the empirical relation by Sekanina (1981b)

$$\frac{1}{v_{gr}} = a + \frac{b}{\sqrt{\beta}}, \quad (2)$$

where a and b are coefficients which depend on the velocity of the gas driving the dust, dust and gas production rates, nature of the dust grain, and the nuclear radius. Sekanina and Larson (1984) have used this equation, with success, for dust emission from discrete sources and pointed out that the linear relation between $(1/v_{gr}, 1/\sqrt{\beta})$ in Eq. (2) is valid for grains with $\beta \leq 0.6$ with slightly absorbing grains. Here we assume β to vary between 0.03 and 0.8 and that Probstein's approach is applicable.

3.2. The Geometry

Details of the geometry to calculate the sky plane coordinates of the dust grains with respect to the comet are discussed by one of us elsewhere (Vasundhara 1999). The basic steps are given in the following sections. The geometry is shown in Fig. 1. The ascending node of the comet's equator on the Earth's equator is N_{equ} and that on the ecliptic is N_{ecl} . The points S and E are the sub-Sun and sub-Earth points, respectively, and N_C is the comet's north pole. The vector v_{gr} is the ejection velocity of the grain and α the acceleration due to solar radiation pressure.

3.2.1. Comet-o-centric spherical coordinates referred to the comet's equator. In the simulation, we follow the track of the dust grain ejected from an active region $G(u, \phi, R, t=0)$ at longitude u and latitude ϕ on the surface of a spherical nucleus of radius R in the comet-o-centric frame referred to the comet's

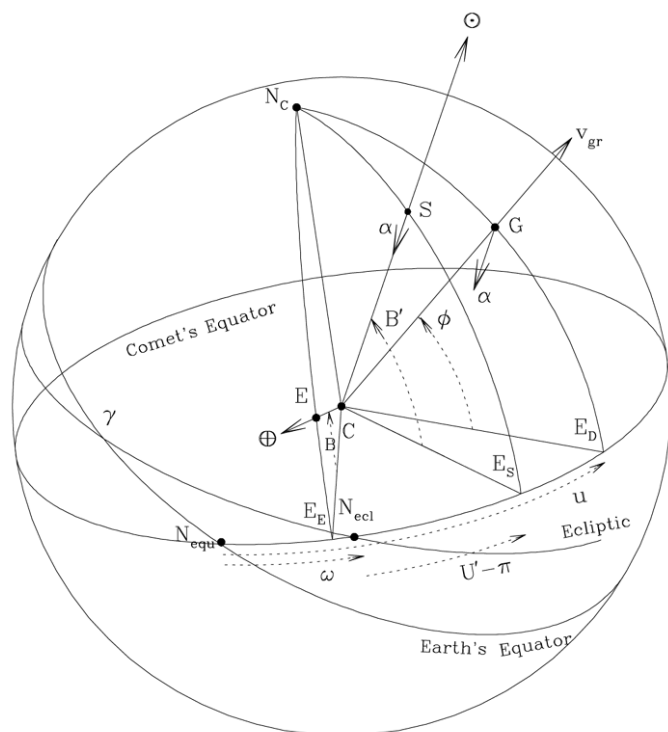


FIG. 1. Geometry indicating the location of the source G and the directions of the initial velocity v_{gr} and acceleration α of the ejected grain. The sub-Sun point, sub-Earth point, and the North pole of the comet are S , E , and N_C , respectively.

equator (Fig. 1). The longitude is measured along the direction of rotation of the comet from N_{equ} . Relative to the comet, during time t , the dust traverses a distance $v_{\text{gr}}t$ radially outward from the comet and a distance $1/2\alpha t^2$ along the Sun–comet direction due to solar radiation pressure. Since the comet-o-centric distances of the shells are much larger than the size of the nucleus, the longitude u' , latitude ϕ' , and radial distance $r'(u', \phi', r', t = t)$ of the grain at time t measured from the instant of ejection are given by

$$\begin{aligned} r' \cos \phi' \cos u' &= v_{\text{gr}}t \cos \phi \cos u - (1/2)\alpha t^2 \cos B' \cos U'' \\ r' \cos \phi' \sin u' &= v_{\text{gr}}t \cos \phi \sin u - (1/2)\alpha t^2 \cos B' \sin U'' \\ r' \sin \phi' &= v_{\text{gr}}t \sin \phi - (1/2)\alpha t^2 \sin B', \end{aligned} \quad (3)$$

where U'' is the longitude of the sub-Sun point S measured from N_{equ} and B' , the comet-o-centric latitude of the Sun. From Fig. 1, it is easy to see that

$$U'' = \omega + U' - \pi,$$

where $U' - \pi$ is the comet-o-centric longitude of the Sun measured along the direction of rotation of the comet from N_{ecl} , and w is the distance of N_{ecl} from N_{equ} , both points being on the equatorial plane of the comet. The expressions in Eq. (3) are strictly valid only if α is constant in direction and magnitude. A constant value of α may be a reasonably good approximation in the present case as we fit only a maximum of eight shells ejected during a time span of about 90 h.

3.2.2. Comet-o-centric spherical coordinates referred to the earth's equator. The comet-o-centric coordinates (u', ϕ', r', t) of the grains referred to the comet's equator were then transformed to the comet-o-centric spherical coordinates with respect to the Earth's equator (A, D, r', t) , where A and D are the comet-o-centric right ascension and declination of the grain. This transformation depends on the right ascension α_p and declination δ_p of the pole of the comet. The inclination of the comet's equatorial plane to the Earth's equator is given by $J = \pi/2 - \delta_p$, and the position of the node N_{equ} is given by $N = \alpha_p + \pi/2$. The comet-o-centric latitude of the Earth B , the position angle of the projection of the north pole of the comet on the sky plane P , and the angles B' and U' were calculated utilizing the equations used for calculating the planet-o-centric positions of the satellite with respect to the planets (Rhode and Sinclair 1992).

3.2.3. Transformation to geocentric spherical coordinates. In the comet-o-centric Earth's equatorial frame, position of the Earth is specified by the distance Δ , right ascension $\alpha_c + \pi$, and declination $-\delta_c$, and that of the grain as (A, D, r') , where $(\alpha_c, \delta_c, \Delta)$ are the geocentric spherical coordinates of the comet. The geo-centric spherical coordinates of the grain (α_g, δ_g) were calculated from A, D, r', α_c , and δ_c utilizing the rigorous expressions involving the comet-o-centric Earth's equatorial coordinates of the sub-Earth point and the grain (Gurnette and Woolley 1960). These equations, meant for computing the differential coordinates of satellites (here the grain) with respect

to the primary (comet), do not make any assumptions regarding the latitude of satellites and hence are directly applicable in the present case of the comet-dust geometry.

4. FIT OF THE OBSERVATIONS TO THE MODEL

The differential coordinates of the dust grains with respect to the comet center on the simulated shell, $\Delta\alpha_g \cos \delta_g = (\alpha_g - \alpha_c) \cos \delta_g$ and $\Delta\delta_g = \delta_g - \delta_c$, depend on the pole positions, location of the sources on the comet (Eq. (3)), the parameter β of the grain, and its velocity v_{gr} given by Eq. (2). The simulated jet and shell structures were fitted with the observed structures by iteratively adjusting these parameters. In order to limit the computer file size of the simulated plots, the longitude sampling was selected between 5° and 30° . Such a discrete sampling however produces radial streaks in the 1996 and October 1997 images instead of a more realistic continuous surface of the ejection cones.

4.1. Pole Position of the Comet and Latitude of the Active Sources

In the images of February–May 1997, sets of shells were fitted with computer-synthesized patterns. At distances of about 3 AU and with seeing discs of about 2 arcsec, the helical structure due to the diurnal motion of the comet in the 1996 and October 1997 images are not discernible. For these images, pairs of jets were recognized as the projected boundaries of cones of jets generated by the rotating sources (Sekanina and Boehnhardt 1997) and these were fitted. The fits were determined by visual matching between the images and the computed structures after superposing them. Separation between the shells depends on the orientation of the line of sight to the equatorial plane (i.e., the comet-o-centric latitude B), the latitude of the source, velocity, and acceleration of the grains determined by the parameters a and b in Eq. (2). Orientation of shells depends on P and is modified by the direction of solar radiation pressure. The first step in comparison was carried out by varying (α_p, δ_p) as well as the latitude of sources in order to simultaneously match the orientation of various shells. Even though a variety of combinations of α_p and δ_p values yield the desired position angle P , the corresponding values of B differ. Again, the same shell pattern could be generated by different combinations of B and ϕ . We attempted to resolve this ambiguity by assuming that the same sources were active (if sunlit) in images taken 1–2 months apart. After about two iterations the pole positions and the source latitudes could be constrained within $\pm 5^\circ$. An optimal solution was selected which reasonably fitted all the observed sets of shells. Fitted pole positions are given in Table II. The best-fitting comet-o-centric latitude of the sources are given in Table III. Although no deliberate attempt was made to place the sources at symmetric latitudes, the best fit shows a remarkable symmetry. The sources that appeared to be active on the dates of our observations are shown in Fig. 2. Since the fits were carried out interactively by visual inspection, the uncertainties in the computed values of the pole positions and the latitudes indicate the range over which the fits appeared good and remained

TABLE II
The Pole Positions and the Geometry

| Date | $\alpha_p(2000)$ (deg) | $\delta_p(2000)$ (deg) | P (deg) | B (deg) | B' (deg) | I (deg) | Φ (deg) |
|--------------|---------------------------|---------------------------|--------------|--------------|---------------|--------------|-----------------|
| 1996 Oct. 06 | 270 | -60 | 175 | -34 | -32 | 80 | 78 |
| 1996 Nov. 04 | 260 | -65 | 183 | -28 | -21 | 77 | 84 |
| 1997 Feb. 18 | 290 | -60 | 189 | -03 | 22 | 90 | 78 |
| 1997 Apr. 10 | 283 | -63 | 216 | 49 | 84 | 87 | 81 |
| 1997 May 02 | 285 | -55 | 210 | 51 | 62 | 88 | 73 |
| 1997 Oct. 09 | 267 | -50 | 158 | -06 | -01 | 77 | 68 |

TABLE III
Longitude and Latitude of the Active Regions

| Latitude ($\pm 05^\circ$) Date | +65° | +35° | +5° | -5° | -35° | -65° |
|-------------------------------------|------------------------|--------|-----|-------|------|--------|
| | Longitude (± 38) | | | | | |
| 1997 Feb. 18 | 111 | 174 | 151 | 359 | 252 | 75 |
| 1997 Apr. 10 | 142 | | 58 | 26 | | |
| 1997 May 02 | 332 | | 271 | 157 | | |
| Color code | Magenta | Purple | Red | Green | Cyan | Yellow |

indistinguishable. The derived latitudes for two of the sources and the pole positions on common dates differ from our earlier preliminary estimates by $\leq 20^\circ$ (Vasundhara *et al.* 1999). The computed values of argument of the subsolar meridian at perihelion Φ and the obliquity I (Sekarina 1981a) corresponding to the fitted pole position of the date are given in Table II.

4.2. The Coefficients a and b

After the orientation and shape of the shells were matched, the coefficients a and b in Eq. (2) were allowed to vary, in order to match the separation between the individual shells. The parameter a determines the mean grain velocity and b the velocity dispersion and hence the width of the shells. Reliable estimates of the parameter b can only be made by including the entire range of grain sizes which can be detected in the visible region. In the

present investigation, for fitting 4–6 shells, grains with β values of 0.03, 0.06, 0.1, 0.2, 0.3, 0.4, 0.5, 0.6, and 0.8 were found to be adequate. Heavier grains fall behind and the lighter grains are swept away by solar radiation pressure. A quantitative modeling by incorporating the scattering efficiency of the grains and a realistic size distribution of the grain population will be needed to reliably match the observations. Finite size of the source will also contribute to the width of the shells. A point source assumption and forcing the fit by adjusting only b in Eq. (2) will overestimate this parameter. Further, sorting of grains of different compositions will lead to branching in the older shells (Sekarina 1981b). Spreading of finer dust grains due to surface breeze (Huebner *et al.* 1986) may cause smearing effects which will influence the estimates of b . Changes in the grain size with time due to possible splitting or grain evaporation could lead to variation in the width of successive shells. All these effects are difficult to model and further, since the fits were carried out by

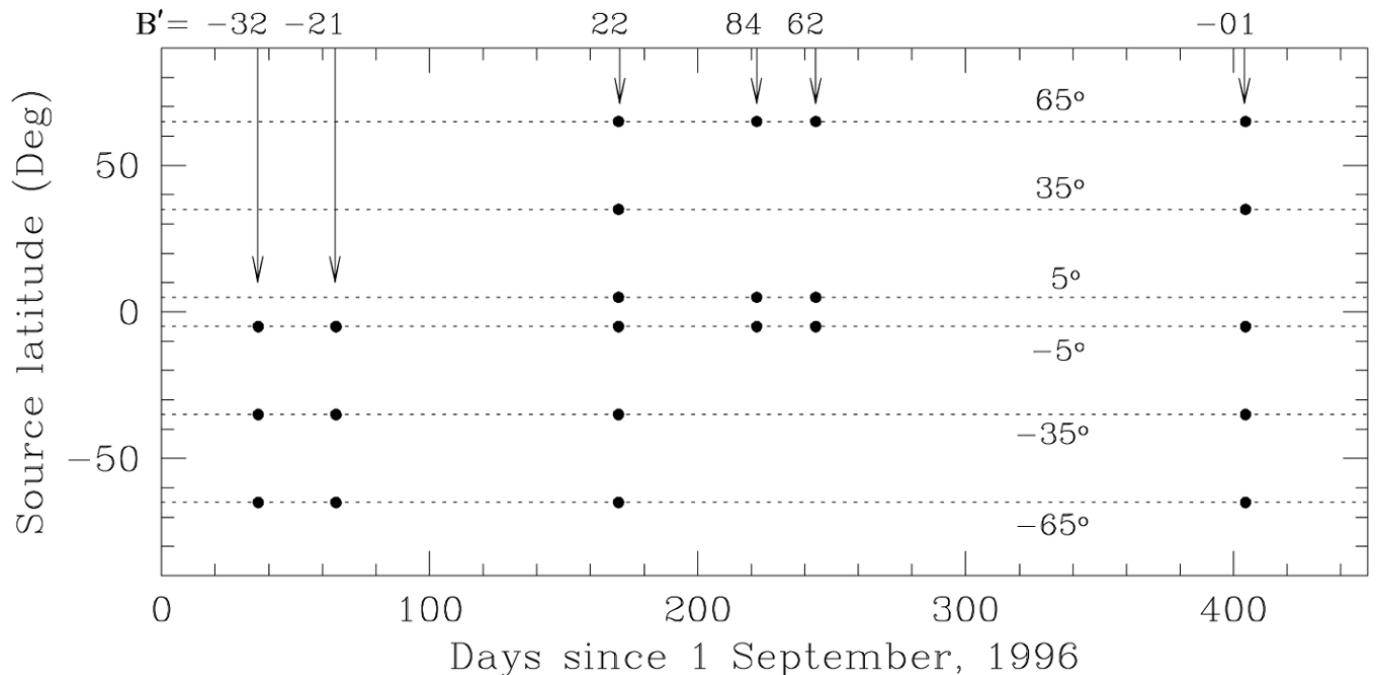


FIG. 2. Fitted latitudes of the active regions on 6 October and 4 November, 1996, 17 February, 10 April, and 2 May 1997. During late 1996, the solar illumination on the southern side ($B' < 0^\circ$) activated the southern sources, while the northern and near-equatorial sources were active during April–May 1997 ($B' > 0^\circ$).

TABLE IV
Lower Limits on Gas and Dust Production Rates

| Date | a s/km ± 0.1 | b s/km ± 0.05 | Dust loading Ψ | Production Rates | | r AU | v_g km s^{-1} |
|--------------|--------------------------|---------------------------|---------------------------|--|--------------------------|-----------|-----------------------------|
| | | | | Gas $\dot{\mu}$ $10^{-5} \text{ g cm}^{-2} \text{ s}^{-1}$ | Dust $\Psi \dot{\mu}$ | | |
| 1997 Feb. 18 | 1.85 | 0.15 | 4.8 ± 1.1 | 2.2 ± 1.5 | 10.6 ± 2.4 | 1.175 | 0.535 |
| 1997 Apr. 10 | 1.50 | 0.13 | 3.4 ± 1.0 | 2.6 ± 2.0 | 9.0 ± 2.7 | 0.932 | 0.601 |
| 1997 May 02 | 1.90 | 0.15 | 6.2 ± 1.3 | 2.1 ± 1.4 | 13.1 ± 2.8 | 1.069 | 0.561 |

visual inspection, the estimated values of the parameter b may have large uncertainties. For this reason, no attempt was made to fit a and b values separately for each source. For the 1996 images and the October 9, 1997, image, the individual shell structures are not resolved. The uncertainty in estimation of a and b is further degraded for these dates as these were derived by matching the observed curvature of the jet pairs. Hence the best fitting values of these coefficients only for the data of February–May are given in Table IV. The uncertainties in the fitted parameters relate to the range over which the fits appeared good.

4.3. Longitude of the Active Sources

The program computes n shells ejected $t = n \times T + dt$ days previously, where T is the period of rotation of the comet. We take dt to be zero when the source crosses the meridian through the sub-Earth point. The parameter dt was adjusted to slide the computed features in the projected radial direction with respect to the comet center. The fitted value of dt permits us to determine the longitude λ of the sources. Following Sekanina and Larson (1984) we measure the longitude along the equator of the comet from the meridian of the subsolar point at perihelion. Lack of the resolved spiral structure in the 1996 and the October 1997 images precluded longitude estimates. The estimated values of (λ, ϕ) for the February–May 1997 images are given in Table III. Uncertainties in the longitude estimates are directly linked with the uncertainties in the fitted parameters a and b . In the present study, the required shift dt could only be determined to an accuracy of 0.05 days. The derived longitudes therefore have an uncertainty of $\pm 38^\circ$. The longitude of the three sources at $\phi = +65^\circ$, $+5^\circ$, and -5° , active between 18 February and 2 May, 1997, are plotted in Fig. 3. No information on the possible movement of the node of the comet’s equator on its orbit or reliable correlation between the longitudes of the three sources can be deduced owing to limited data.

5. RESULTS AND DISCUSSIONS

5.1. The Fitted Images

The observed structures are compared with the simulations in Fig. 4. The left and middle panels show the observed processed images and the simulated structures, respectively. These

two are superposed in the right panels to enable critical comparison. The color codes for jets from different latitudes are given in Table III. The projected comet–Sun radius vector is indicated by the arrow. No attempt was made to match the intensity of the shells. In order to simulate the hazy features consisting of finer grains with $\beta > 0.8$ in the projected anti-Sun direction, the simulated plots contain in addition, points representing grains with β values of 1.2, 1.5, 1.8, and 2.5. Since very small grains with radii less than $1 \mu\text{m}$ attain nearly constant velocities (Gombosi 1986, Delsemme 1982), with sufficient accuracy, the velocity of these smaller grains were assigned the value corresponding to $\beta = 0.8$. Each simulated shell thus contains 13 points. Ideally, the number of points of a given grain size should be governed by a power law distribution (Hanner 1983, Sekanina 1998a). In the present work, except for the end points, we have sampled β values of equal interval between 0.1 and 0.6. Since $\beta \propto 1/s$

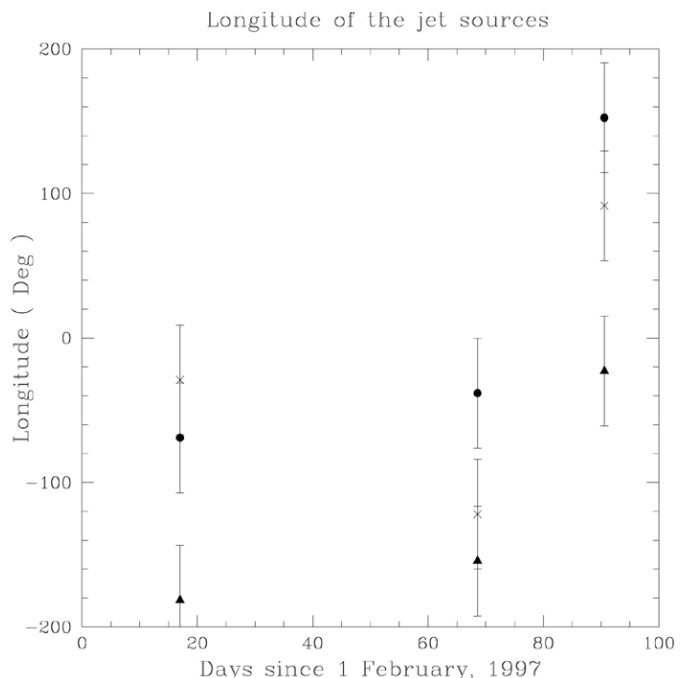


FIG. 3. Longitude of the sources on 17 February, 10 April, and 2 May 1997. Filled circles, crosses and filled triangles represent sources at latitudes $+65^\circ$, $+5^\circ$, and -5° , respectively.

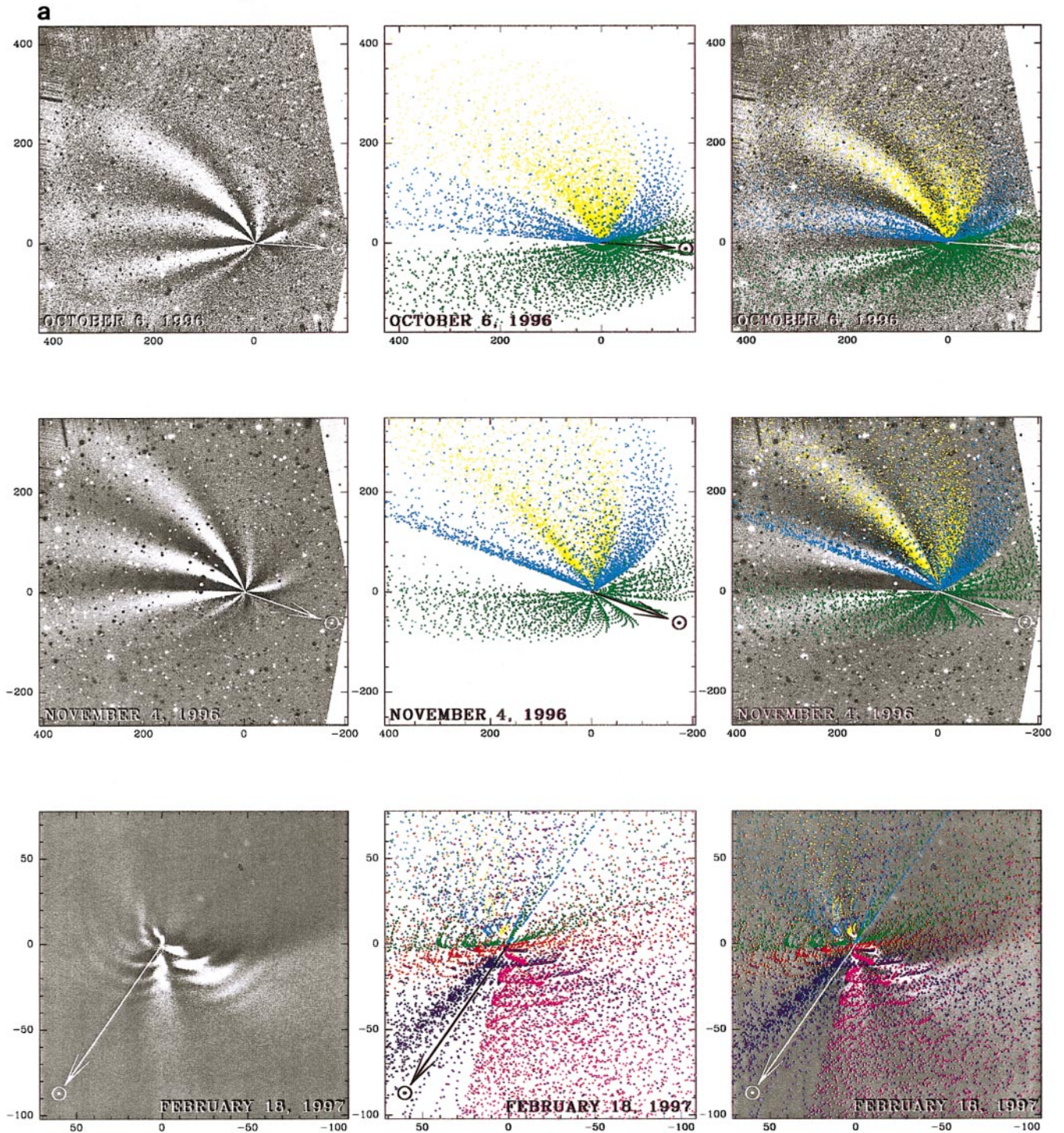


FIG. 4. (a) Fit of the model to the preperihelion images. In each row, the left panel shows the observed processed image and the middle panel shows the simulated structures. On the right panel, both observed and simulated structures are superposed. The β values of the grains range between 0.06 and 2.5. The projected direction of the Sun is indicated by the arrow. North is up and east is to the left. The scales are in arcsec centered on the comet. Color codes for ϕ are: $-65^\circ = \text{Yellow}$, $-35^\circ = \text{Cyan}$, $-5^\circ = \text{Green}$, $+5^\circ = \text{red}$, $+35^\circ = \text{Purple}$ and $+65^\circ = \text{Magenta}$. (b) Fit of the model to the postperihelion images. Other details are the same as those for (a).

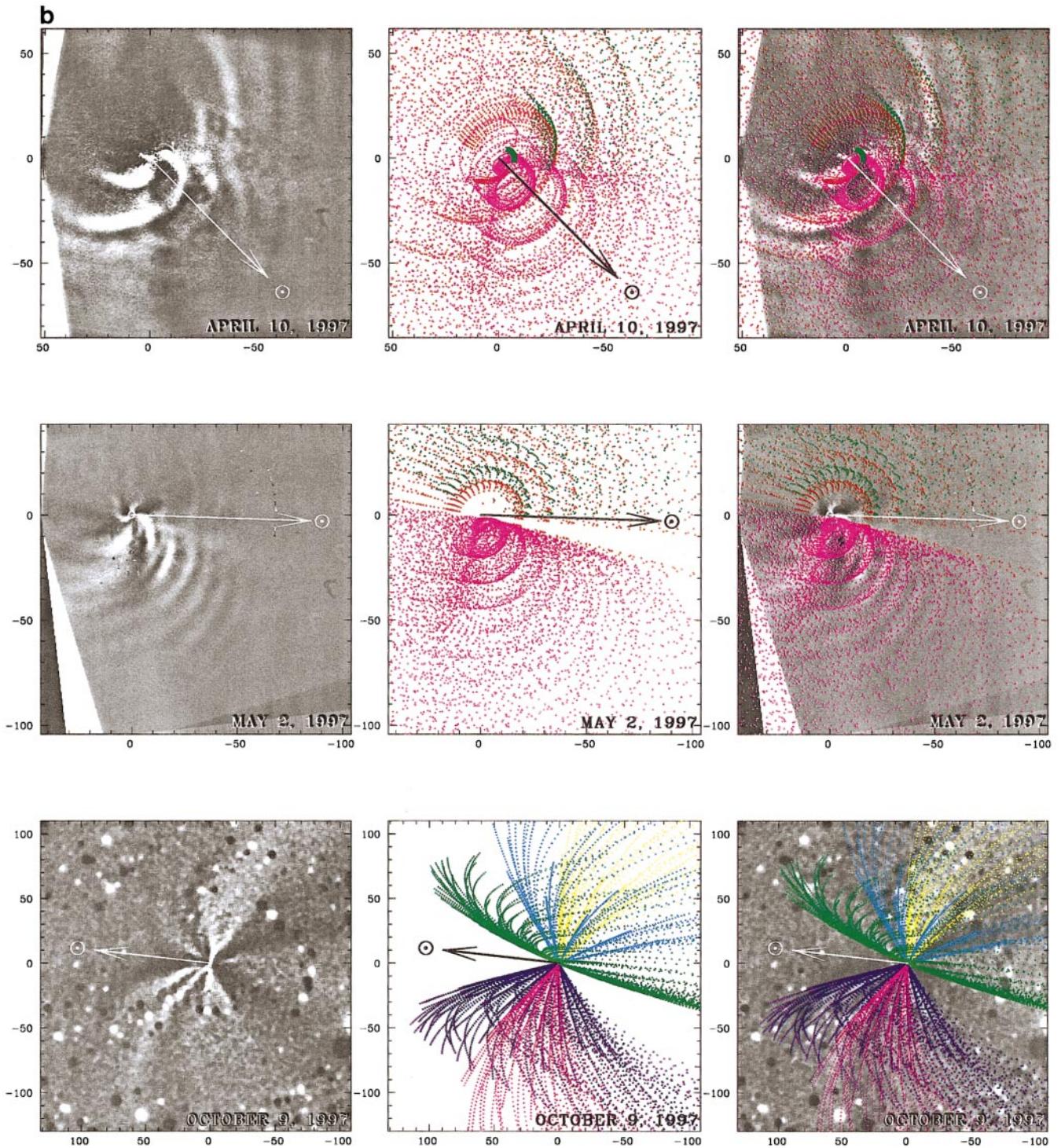


FIG. 4—Continued

(Finson and Probstein 1968), where s is the radius of the grain, such a sampling of β results in over sampling of smaller grains mimicking a s^{-2} law. Further, in the simulated image, contributions of grains of all sizes are represented by dots of the same

size. The number of grains a dot represents is therefore proportional to s^{-2} . Thus the simulated pattern with the sampling of β value discussed above represents approximately a power law distribution with an index of ≈ -4 .

5.2. Gas and Dust Production Rates

Sekanina and Larson (1984) have shown that for Comet Halley outbursts in 1910, the linearity of Eq. (2) was satisfied for $\beta \leq 0.6$. We relaxed this restriction on β to 0.8 to simulate the extensions of the shells along the projected anti-Sun direction consisting of finer grains. We used the following equations used by these authors to calculate the lower limit on the mass loading by dust Ψ and the gas production rate $\dot{\mu}$ corresponding to an upper limit of 0.8 for β

$$\Psi > 5.0 \left[3av_g \left[1 - \frac{0.65}{1.65 + 8.5(bv_g)^{4/3}} \right] - 1 \right]^{5/3} \quad (4)$$

$$\dot{\mu} > 0.93 \times 10^{-5} / Rb^2 v_g.$$

The nuclear radius R was taken to be 35 km, the upper limit by Weaver and Lamy (1999) and Sekanina (1999b). The thermal velocity of the gas v_g at heliocentric distance r was calculated using the relation by (Delsemme 1982)

$$v_g = 0.58r^{-0.5}. \quad (5)$$

The estimated lower limits on production rates of gas and that of the dust using the fitted values of a and b are given in Table IV along with the heliocentric distance of the comet and the gas velocity v_g . If water constitutes 80% of the total gas production, the lower limit on the gas production rate $\dot{\mu}$ in April 1997 estimated in the present work of $2.6 \times 10^{-5} \text{ g cm}^{-2} \text{ s}^{-1}$ (Table IV), yields a lower limit on the evaporation rate of water of $7 \times 10^{17} \text{ molecules cm}^{-2} \text{ s}^{-1}$. This is 35% of the upper limit on the production rate of about $20 \times 10^{17} \text{ molecules cm}^{-2} \text{ s}^{-1}$ (Delsemme 1982) expected at the heliocentric distance of 0.93 AU for normal incidence of sunlight for a zero albedo surface. Extension of the range of the grain sizes compared to our earlier study (Vasundhara *et al.* 1999) has improved the estimates of the parameter b and hence the gas production rates. This estimate can be further improved if a quantitative fit is carried out for the estimation of the parameter b taking into account the finite size of the jet sources. As mentioned in Section 4.2, the finite size assumption may result in the over estimate of the parameter b and an under estimate of $\dot{\mu}$.

5.3. Activity of the Various Sources

Gradual changes in the appearances of the dust shells from the comet with time can be understood in terms of the varying Earth-comet geometry and changes in the comet-o-centric latitude of the Sun (B') which determines activation of sources at different latitudes and fractional period of their activity. A large value of the comet-o-centric latitude of the Earth B in April permitted a high-latitude view of the sets of concentric rings and arcs elongated in the projected anti-Sun direction. It is interesting to note that the source at $+35^\circ$, which was apparently active during February 1997 to March 1997 (Vasundhara *et al.* 1999), ceased to be active in April in spite of the high northern (cometary)

latitude of the Sun. Activity of a source near this latitude is again seen in the image of the comet taken in October 1997 when the comet-o-centric latitude of the Sun was near zero. If the pre- and postperihelion features are from the same source, one of the reasons for its inactivity during April–May 1997 may be local shadowing, possibly by an overhanging mountain ridge north of this source. This explanation is supported by the fact that the activity from this source was noticed to resume again when the solar illumination became near equatorial (e.g., October 1997 image).

5.4. Size of the Sources

During early April 1997, three sets of shell structures are inferred from the present analysis (Table III). One from the high-latitude active source at $+65^\circ$ and the two near equatorial sources at $+5^\circ$ and -5° . On April 10, the rotation averaged values of the cosine of the Sun's zenith distance ($\langle \cos z_\odot \rangle$) as seen by these sources were 0.913, 0.092, and 0.003, respectively. Schleicher *et al.* (1997) report a total water production rate of $4 \times 10^{30} \text{ molecules s}^{-1}$ from the comet near perihelion. To assess the contribution from these sources to the observed water production rate during early April, it may be noted that the equatorial sources were illuminated by the Sun at near-grazing incidence and that the source at $+65^\circ$ must be small in size. The constraint on the size of the high-latitude source is evident because the total area north of the latitude ϕ for a spherically symmetric comet is given by $0.5(1 - \sin \phi)$ of the total surface area of the comet (Sekanina 1987). If we assume that this source spans between 60° and 70° in latitude, the total area between the two latitude circles is 567 km^2 . The observed well-defined shells from this source due to the diurnal variation cannot be explained if this source occupies a substantial fraction of this area. Assuming that the source occupies 36° in longitude, the total production of water from this source will be $11.4 \times 10^{29} \text{ molecules s}^{-1}$. This is 29% of the total observed production rate. In spite of the near-grazing incidence of sunlight, the shells from the equatorial sources appear comparable in intensity to the high-latitude source at $+65^\circ$. Further, the shells from -5° and $+5^\circ$ are not resolved in any of the images between February and May. Hence it is likely that a single source or a source complex stretches from -5° to $+5^\circ$. It is difficult to comprehend the reason for the near equal brightness of the two sets of shells when the values of ($\cos z_\odot$) at the respective sources differed by a large factor. Further, the best fitting pole position for the shells from the source at $+65^\circ$ does not yield a very good fit for the equatorial shells during April (Fig. 4b). The interwoven shells observed during February 1997 appear too complex to be explained using a single nucleus. The 10 April 1997 image shows two sets of shell structures. While the high-latitude source at 65° explains the shells (magenta) expanding in the southwesterly direction, we found it impossible to fit the near equatorial shell with a single source corresponding to the apparent anticlockwise rotation of the nucleus during April. We have therefore invoked two sources, one at $+5^\circ$ latitude producing the shell structures

(colored red) SE of the nucleus and another at -5° to produce the shells (colored green) NW of the nucleus. In spite of best efforts, even this bimodal matching is not perfect. The observed shells have less curvature compared to the simulated shells. Further, if the activity of the source at $+5^\circ$ had continued until sunset as per our assumptions, the longitudinal extent of the shells in the simulated image should have continued until the NE across the N point. But the region NE of the nucleus is devoid of any shell structure. The projected comet-o-centric separation of the observed shells in the NW and SE corresponding to a given diurnal cycle match better for a clockwise motion of the source and in such a case, a single source can explain the observed feature. The curvature of these equatorial shells could be adjusted with a separate pole solution. Thus there appears to be the need for two separate bodies with opposite senses of rotations, one hosting the high-latitude source and the other the near-equatorial source. This is in conformity with the binary model by Sekanina (1998b) with the two nuclei having their spin vectors subtending an angle $>90^\circ$ with each other to explain the complex shell structures in the images of late February 1997 and late March 1997. In order to explain the constant phase difference between the two sets of shell patterns, the two components must have nearly the same synodic period. The binary scenario is also in conformity with the reported differences in color and polarization of the two sets of shells by Jockers *et al.* (1999).

6. CONCLUSIONS

Although the observations could be reasonably matched with the simulations, the present model assuming a single nucleus does not however replicate the exact shapes of the shells and the complex observed shell patterns. Detailed modeling taking into account the binary nature of the comet (Sekanina 1999a and 1998b) may be required to explain the observed intricate shell structures. The pole positions during the one-year period of observations are found to vary between 260° and 290° in right ascension and -50° to -65° in declination, indicating a complex state of rotation of the comet. The present data set is insufficient to draw a meaningful conclusion on the possible precession or complexity of the rotation of the comet. The derived pole positions compare well with the reported values of $\alpha_p = 257^\circ$ and $\delta_p = -61^\circ$ by Sekanina (1998a) for late February 1997 and $\alpha_p = 275^\circ$ and $\delta_p = -57^\circ$ by Jorda *et al.* (1999) for February–March 1997. Our average value of $\alpha_p = 276^\circ$ is close to the value of $\alpha_p = 270^\circ$ corresponding to the ecliptic longitude of 270° and latitude of -20° pertaining to a complex rotational state of the nucleus with a small precessional angle reported by Samarasinha *et al.* (1999). The latitude of the northern most source of 65° derived in the present study is in conformity with the value of $64 \pm 5^\circ$ reported by Jorda *et al.* (1999). The average value of dust to gas production ratio between February 1997 and May 1997 is found to be near 5. During April, the source at $+65^\circ$ appears to account for about 29% of the observed total water emission reported by Schleicher *et al.* (1997). In addi-

tion, several smaller jet sources not delineated in Figs. 4a and 4b, distributed sources of water from evaporation of the grains in flight and outgassing from the inactive regions of the comet may contribute to the total observed water production rate.

ACKNOWLEDGMENTS

One of us (P.C.) thanks Prof. M. A'Hearn for useful discussions on the application of rotational shift algorithm to the images. We are extremely grateful to the two referees, Dr. N. Samarasinha and Prof. Z. Sekanina for their valuable comments.

REFERENCES

- Delsemme, A. H. 1982. Chemical composition of cometary nuclei. In *Comets* (L. L. Wilkening, Ed.), pp. 85–130. University of Arizona Press, Tucson.
- Finson, M. L., and R. F. Probstein 1968. A theory of dust comets. I. Model and equations. *Astrophys. J.* **154**, 327–352.
- Gombosi, T. I. 1986. A Heuristic model of the Comet Halley dust size distribution. In *Proc. 20th ESLAB Symposium on the Exploration of Halley's Comet*, pp. 167–171. ESA SP-250.
- Gurnette, B. L., and R. v. d. R. Woolley (Eds.) 1960. In *Explanatory Supplement to the Astronomical Ephemeris and The American Ephemeris & Nautical Almanac*, pp. 342–397. Prepared by the Nautical Almanac Offices, UK and USA.
- Hanner, M. S. 1983. The nature of cometary dust from remote sensing. In *Cometary Exploration* (T. I. Gombosi, Ed.), Vol. 2, pp. 1–22. Central Research Institute for Physics Press, Budapest.
- Huebner, W. F., H. U. Keller, K. Wilhelm, F. L. Whipple, W. A. Delamere, H. J. Reitsema, and H. U. Schmidt 1986. Dust–gas interaction deduced from Halley multicolour camera observations. In *Proc. 20th ESLAB Symposium on the Exploration of Halley's Comet*, pp. 363–364. ESA SP-250.
- Jockers, K., V. K. Rosenbush, T. Bonev, and T. Credner 1999. Images of polarization and colour in the inner coma of Comet Hale–Bopp. *Earth Moon Planets*, in press.
- Jorda, L., K. Rembor, J. Lecacheux, P. Colom, F. Colas, E. Frappa, and L. M. Lara 1999. The rotational parameters of Hale–Bopp (C/1995 O1) from observations of the dust jets at Pic du Midi Observatory. *Earth Moon Planets*, in press.
- Larson, S. M., and Z. Sekanina 1984. Coma morphology and dust-emission pattern of periodic Comet Halley. I. High resolution images taken at Mount Wilson in 1910. *Astron. J.* **89**, 571–578.
- Licandro, J., L. R. B. Rubio, H. Boehnhardt, R. Casas, B. Göetz, A. Gómez, L. Jorda, M. R. Kidger, D. Osip, N. Sabalisk, P. Santos, M. Serra-Ricart, G. P. Tozi, and R. West 1998. The rotation period of C/1995 O1 (Hale–Bopp). *Astrophys. J.* **501**, L221–L225.
- Manzini, F., C. Guaita, and F. Crippa 1996. *IAU Circ.* **6463**.
- Probstein, R. F. 1969. In *Problems of Hydrodynamics and Continuum Mechanics* (F. Bisshopp *et al.*, Eds.), pp. 568–583. Soc. Industr. Appl. Math.
- Rhode, J. R., and A. Sinclair 1992. Orbital elements and rings of satellites. In *Explanatory Supplement to the Astronomical Almanac* (P. K. Seidelmann, Ed.), pp. 325–381. Nautical Almanac Offices, UK and USA, Jet Propulsion Laboratory, Bureau des Longitudes and the Time Service and Astrometry departments, U.S. Naval Observatory.
- Samarasinha, N. H., B. E. A. Mueller, and M. J. S. Belton 1999. Coma morphology and constraints on the rotation of Comet Hale–Bopp (C/1995 O1). *Earth Moon Planets*, in press.
- Schleicher, D. G., R. L. Millis, T. L. Farnham, and S. M. Lederer 1997. Results from narrow band photometry of Comet Hale–Bopp (1995 O1). *Bull. Am. Astron. Soc.* **29**, 1033.

- Sekanina, Z. 1981a. Rotation and precession of cometary nuclei. *Annu. Rev. Earth Planet. Sci.* **9**, 113–145.
- Sekanina, Z. 1981b. Distribution and activity of discrete emission areas on the nucleus of periodic Comet Swift–Tuttle. *Astron. J.* **86**, 1741–1773.
- Sekanina, Z. 1987. Anisotropic emission from comets: Fans versus jets. II. Periodic Comet Tempel 2. In *Proc. Symposium on the Diversity and Similarity of Comets* (E. J. Rolfe and Battryck, Eds.), pp. 323–336. ESA SP-278.
- Sekanina, Z. 1991. Cometary activity, discrete outgassing areas, and dust-jet formation. In *Comets in the Post-Halley Era* (R. L. Newburn, Jr., M. Neugebauer, and J. Rahe, Eds.), pp. 769–823. Kluwer, Dordrecht/Norwell, MA.
- Sekanina, Z. 1996. Activity of Comet Hale–Bopp (1995 O1) beyond 6 AU from the Sun. *Astron. Astrophys.* **314**, 957–965.
- Sekanina, Z. 1998a. Modeling the diurnal evolution of a dust feature in Comet Hale–Bopp (1995 O1). *Astrophys. J.* **494**, L121–L124.
- Sekanina, Z. 1998b. Modeling dust halos in Comet Hale–Bopp (C/1995 O1): Existence of two active nuclei unequivocally implied. *Astrophys. J.* **509**, L133–L136.
- Sekanina, Z. 1999a. Detection of a satellite orbiting the nucleus of Comet Hale–Bopp (C/1995 O1). *Earth Moon Planets*, in press.
- Sekanina, Z. 1999b. A determination of the nuclear size of Comet Hale–Bopp (C/1995 O1). *Earth Moon Planets*, in press.
- Sekanina, Z., and H. Boehnhardt 1997. *IAU Circ.* **6542**.
- Sekanina, Z., and H. Boehnhardt 1999. Dust morphology of Comet Hale–Bopp (C/1995 O1). II Introduction of a working model. *Earth Moon Planets*, in press.
- Sekanina, Z., and S. M. Larson 1984. Coma morphology and dust emission pattern of periodic Comet Halley. II. Nucleus spin vector and modeling of major dust features in 1910. *Astron. J.* **89**, 1408–1425.
- Vasundhara, R. 1999. A photometric-dynamic model to simulate jets from comets. Application to Comet Hale–Bopp (C/1995 O1). *Astron. Astrophys.*, submitted.
- Vasundhara, R., P. Chakraborty, A. Hänel, and E. Heiser 1999. Modeling dust jets and shells from Comet Hale–Bopp. *Earth Moon Planets*, in press.
- Weaver, H. A., and P. L. Lamy 1999. Estimating the size of Hale–Bopp’s nucleus. *Earth Moon Planets*, in press.